Available online at www.sciencedirect.com

SciVerse ScienceDirect

Ceramics International 38 (2012) 1267–1273

CERAMICS INTERNATIONAL

www.elsevier.com/locate/ceramint

Effect of sintering temperature on magnetic and electrical properties of nano-sized Co_2W hexaferrites

Mukhtar Ahmad [a], Ihsan Ali [a], Faiza Aen [a], M.U. Islam [a], Muhammad Naeem Ashiq [b], Shabbar Atiq [c], Waheed Ahmad [c], M.U. Rana [a,*]

[a] Department of Physics, Bahauddin Zakariya University, Multan 60800, Pakistan
[b] Department of Chemistry, Bahauddin Zakariya University, Multan 60800, Pakistan
[c] Institute of Advanced Materials, Bahauddin Zakariya University, Multan 60800, Pakistan

Received 26 June 2011; received in revised form 26 August 2011; accepted 27 August 2011
Available online 3 September 2011

Abstract

Nano-sized and single phase W-type hexaferrite ($BaCo_2Fe_{16}O_{27}$) powders synthesized by sol–gel autocombustion method have been investigated. The samples were sintered in a temperature range of 1000–1200 °C for 5 h. The thermal decomposition behavior of as-prepared powder was studied by thermogravimetry (TG), differential thermal analysis (DTA) and infrared spectra (IR). The structural and magnetic properties of powders were investigated by X-ray diffraction (XRD) and vibrating sample magnetometer (VSM). The grain size calculated by Scherer equation was found in the range of 36–47 nm which is small enough to obtain a suitable signal-to-noise ratio in high density recording media. Hysteresis loop measurements show that the coercivity values lie in the range of 210.61–1602.6 Oe with increasing sintering temperature. Magnetization studies show a significant increase in the values from 15 to 22 emu/g. The dc electrical resistivity is observed to decrease up to a certain value as the temperature increases and then rises at higher temperature.

Keywords: Nano materials; W-hexaferrites; IR spectroscopy; X-ray diffraction; Vibrating sample magnetometry; High density recording media

1. Introduction

Ferrites form a very good class of electrical materials because of their high resistivity and low loss behavior, and hence have vast technological applications over a wide range of frequencies [1]. Ferrites assume special significance in the field of electronics and telecommunication industry because of their novel electrical properties which makes them useful in radiofrequency circuits, high quality filters, rod antennas, transformer cores, read/write heads for high digital tapes and other devices [2,3]. In recent years, there has been considerable interest in the study of the properties of nano-sized ferrite particles because of their importance in the fundamental understanding of the physical processes as well as their proposed applications for many technological purposes. The physical properties of the nano materials are predominantly controlled by the grain boundaries than by the grains [4]. The electrical properties of nano ferrites are greatly affected when the particle size approaches to the critical size, below which each particle is treated as single domain [5]. This activity has been inspired in part by the realization that the physical and chemical properties of nano phase materials are in general dramatically different from those of the bulk counter parts and that nano phase materials exhibit new or cross over phenomena [6–8]. Increasing attention has been paid to W-type hexagonal ferrites because their potential application as permanent magnets for electrical, electronic and automobile devices. Also, W-hexaferrites with planar structure are among the most popular microwave absorption materials for their higher efficiency and lower cost than those of other materials [9]. A variety of techniques have been developed to synthesize W-type hexaferrites. The conventional mechanical grinding [10] and glass crystallization methods [11] for W-hexaferrites preparation have disadvantages such as time consuming and introducing impurities into material compositions. Further-

* Corresponding author. Tel.: +92 61 9210199; fax: +92 61 9210068.
E-mail addresses: ahmadmr25@yahoo.com (M. Ahmad), mazharrana@bzu.edu.pk (M.U. Rana).

0272-8842/$36.00
doi:10.1016/j.ceramint.2011.08.059

more, the high calcination temperature (≥1200 °C) results in the formation of coarse aggregation and the vaporization of some compositions. Besides, the calcining temperature is rather high, Zhang et al. [12] have prepared $BaZn_{2-z}Co_zFe_{16}O_{27}$ hexaferrites by citrate sol–gel method, still relatively high calcination temperature of 1100 °C is needed for the formation of W-type hexaferrite phase. Stearic acid gel method has been used to prepare ultrafine W-type hexaferrites, which is a simple method with little limitation except that all raw materials must be dissolved in the molten stearic acid [13]. In this article, we focus on the synthesis of nanocrystalline $BaCo_2Fe_{16}O_{27}$ hexaferrite powders by a sol–gel autocombustion technique, which is a novel way with a combination of sol–gel and the combustion process. This method has the advantage of inexpensive precursor, facile operation, low annealing or sintering temperature, energy-efficiency and the resulting nano-sized particles with narrow size distribution and excellent chemical homogeneity. Moreover the lack of knowledge about temperature dependent magnetic properties of Co_2W-hexaferrites stimulates us to prepare and analyze these nano materials.

2. Experimental

A sample of single-phase polycrystalline W-type hexaferrite of composition $BaCo_2Fe_{16}O_{27}$ has been prepared using the conventional sol–gel autocombustion method. Aqueous solutions of $Ba(NO_3)_2$ (+99%,Sigma Aldrich, Mexico), $Co(NO_3)_2$–$8H_2O$ (+98%, Sigma Aldrich, UK) and $Fe(NO_3)_3$–$9H_2O$ (+98%, Sigma Aldrich, USA) were used. Citric acid (99.91%, Fisher Scientific, UK) was used as a chelating agent. During the synthesis, the aqueous solutions of the metallic salts of the component in stoichiometric ratios and citric acid were slowly added together. The resultant sol was then stirred, using a magnetic stirrer, while being heated at 80 °C, to transform the sol into a gel. Meanwhile pH value of the sol was adjusted to approximately 7–8 by using ammonia (35%, Fisher Scientific, UK). After 6–7 h, the dried gel underwent autocombustion to produce powdered samples. The finely ground powders were pressed into pellets (3.5 mm thickness and 8 mm diameter) under a force of 40 kN for about 1.30 min by using the Paul Otto Webber hydraulic press. Simultaneous sintering of the powders and pellets at a temperature of 1000 °C in a temperature-programmed furnace for 5 h at a heating rate of 12 °C/min resulted in a single-phase W-type hexaferrite. Fig. 1 shows the flow diagram for synthesis of nanocrystalline $BaCo_2Fe_{16}O_{27}$ hexaferrite powders prepared by the above mentioned method. The thermal decomposition behavior of the as-prepared powder was examined simultaneously by means of thermogravimetry (TG) and differential thermal analysis (DTA) with a heating rate of 10 °C/min in the air on the Linsies PT 1600 TGA and DTA instruments, respectively. Infrared (IR) spectra were recorded on Shimadzu 8400S IR spectrometer by KBr pellets method. IR spectra study is specially made to observe the two broad bands, which are characteristic bands of ferrites and usually occur due to tetrahedral and octahedral complexes. X-ray diffraction (XRD) analysis of powder samples were carried out by X-ray

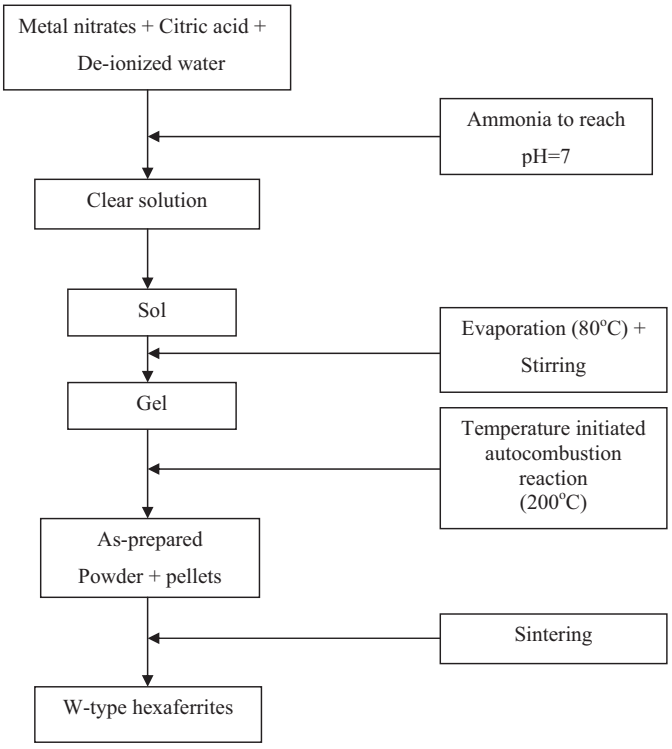

Fig. 1. Flow diagram for synthesis of nanocrystalline $BaCo_2Fe_{16}O_{27}$ hexaferrite powders.

diffractometer equipped with Cu Kα radiation source (λ = 1.5406 Å). The magnetic properties like magnetization values (M) and coercivity (H_c) were measured by a vibrating sample magnetometer (VSM) at an applied field of 8 kOe at room temperature. The bulk density (d_B) was calculated by the relation:

$$d_B = \frac{m}{\pi r^2 t} \quad (1)$$

where 'm', 'r' and 't' are the mass, radius and thickness of the pellet respectively. The dc electrical resistivity was measured by two point probe method at room temperature by the formula;

$$r = \frac{RA}{t} \quad (2)$$

where 'R' is the resistance and 'A' is the area of pellet.

3. Results and discussion

3.1. Thermal analysis

The DT/TGA graph for an as-prepared sample with nominal composition $BaCo_2Fe_{16}O_{27}$ is shown in Fig. 2. The thermal analysis is carried out to evaluate the mechanism for the formation of hexaferrite phase and to observe the effect of heating on structural changes of the synthesized sample. The DTA curve shows a peak at about 100 °C which is due to loss of water from the sample. The other peaks appeared at 291 °C, 526 °C and 920 °C indicating the formation of oxides from hydroxides, monohexaferrite and the formation of hexagonal

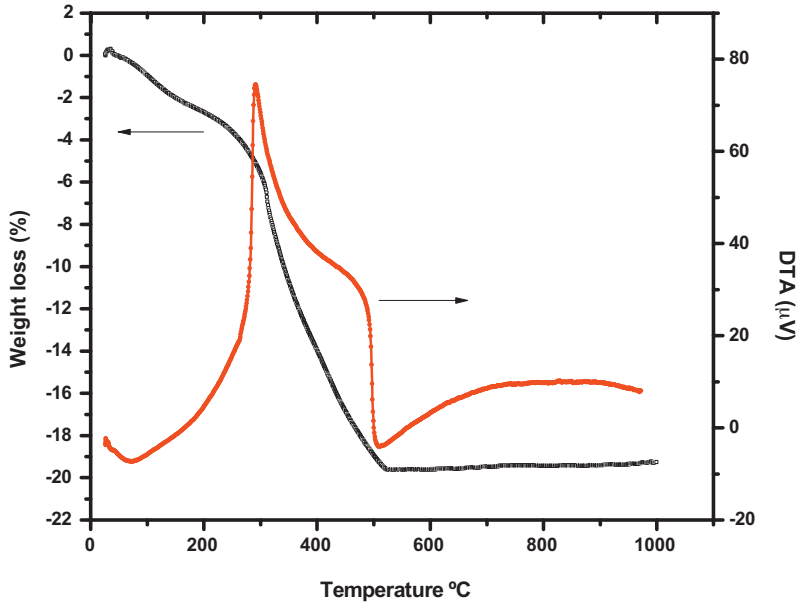

Fig. 2. DT/TGA curve of as-prepared $BaCo_2Fe_{16}O_{27}$ powder.

phase, respectively [14]. Whereas for thermogravimetric curve, two distinct weight loss steps around 100 °C and 291 °C were observed, which were attributed to the decomposition of hydroxides and barium carbonate, respectively.

3.2. FT-IR spectra

The FT-IR spectra of $BaCo_2Fe_{16}O_{27}$ for the as-prepared and sintered (at 1000 °C) samples are shown in Fig. 3(a and b). The spectrum of as-prepared powder shows the characteristic band of O–H stretching vibration of residue water at 3445 cm^{-1}, anti-symmetrical vibration of CO_2^- at about 1581 cm^{-1}, the N–O stretching vibration of NO_3^- at about 1403 cm^{-1} and metal–oxygen stretching vibrations of α-Fe_2O_3 at 549 cm^{-1} respectively [15]. Thus indicating the co-existence of NO_3^- ion, O–H, CO_2^- and iron groups in the as-prepared powder sample. Whereas for sintered samples there are two typical hexaferrite absorption bands, the higher frequency band is seen to be at 588 cm^{-1} and lower frequency band at 431 cm^{-1}. This difference in band position is expected because of difference in $Fe_3^+ - O_2^-$ distance for octahedral and tetrahedral sites. Similar results are observed in chromium substituted ferrite [16].

3.3. Structure determination

Fig. 4 shows the powder XRD patterns of the $BaCo_2Fe_{16}O_{27}$ samples sintered at different temperatures. It is evident from the figure that the sample sintered at 1000 °C is in single phase with hexagonal structure without showing any detectable second phase impurities. The observed diffraction lines were found to compare to those of the standard pattern (ICSD-00-051-1879) of the barium ferrite with no extra line, indicating thereby that all the samples have a single phase hexagonal structure and no unreacted constituents were present in the samples. The FT-IR results are in good agreement with the XRD results. Moreover, on increasing the sintering temperature beyond 1000 °C, broad peaks were observed, which become narrower and sharper at 1200 °C, manifesting the increase of particle size and crystallinity [17].

The lattice parameters (a and c) were calculated from the XRD data using the following equation [18]:

$$\mathrm{Sin}^2\theta = \frac{\lambda^2}{3a^2}(h^2 + hk + k^2) + \frac{\lambda^2}{4c^2}I^2 \quad (3)$$

where 'hkl' are the corresponding indices of each line in the pattern and 'θ' is the Bragg's angle. The observed values of the lattice parameters 'a' and 'c' (a = 5.846 Å, c = 32.854 Å) are in close agreement with the reported values for hexagonal ferrites [19]. The grain size (D) is calculated from diffraction line broadening using the well-known Scherer equation:

$$D = \frac{K\lambda}{\beta\cos\theta} \quad (4)$$

where 'β' is the broadening of diffraction lines at half-width of its maximum intensity, 'λ' is the wavelength (1.5406 A□), and 'K' is a constant (0.89 for hexaferrite). The grain size is found in the range of 36.2–47.01 nm (Table 1). It has been reported that the grain size <50 nm is required to obtain the suitable signal-to-noise ratio in the high density recording media [20]. In the present work the grain size is 36.2–47.01 nm so these materials can be considered to use for applications in high density recording media for obtaining suitable signal-to-noise ratio. The density data of W-type ferrites are given in Table 1. It is seen that as the sintering temperature of ferrites increases, the density increases. But at higher temperature (1200 °C), the density of ferrites decreases which may be due to presence of pores created during sintering process at this temperature. The increase in the density is around 10–11% for a temperature

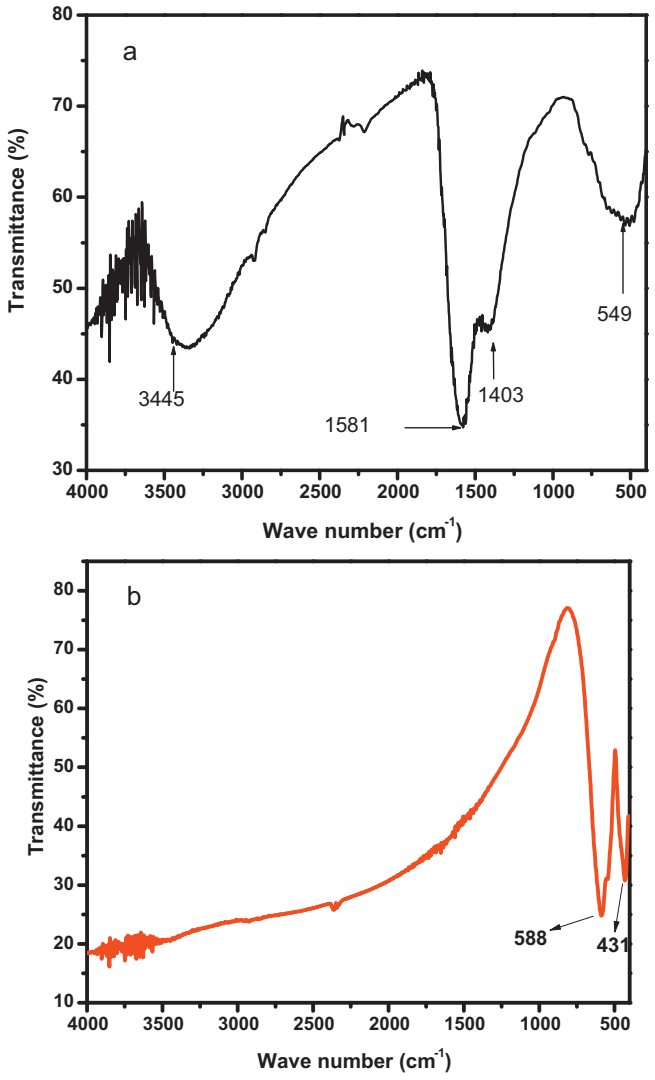

Fig. 3. FT-IR spectra of as-prepared (a) and sintered (b) powders of $BaCo_2Fe_{16}O_{27}$.

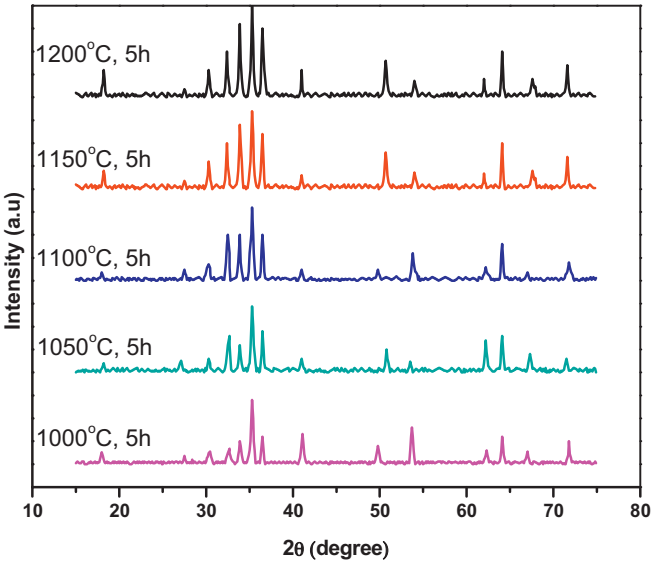

Fig. 4. XRD patterns of $BaCo_2Fe_{16}O_{27}$ powders sintered at different temperatures.

Table 1
Grain size, bulk density, magnetization, magnetic moment, coercivity and resistivity of W-hexaferrite powders at different sintering temperatures.

T (°C)	D (nm)	Density (d_B) (g/cm^3)	M (emu/g)	N_B (μ_B)	H_C (Oe)	ρ (Ω cm $\times$ 10^8)
1000	36.2	3.79	15.52	2.41	1602.6	9.4
1050	37.9	3.98	16.80	2.61	1513.4	8.6
1100	42.9	4.05	18.70	2.90	1133.2	6.2
1150	45.2	4.18	22.02	3.42	210.7	5.1
1200	47.01	4.17	20.12	3.12	210.61	6.3

increase of 150 °C (from 1000 to 1150 °C). There was no significant increase in the density beyond 1150 °C. The maximum density obtained was 4.18 g cm^{-3} at 1150 °C. The behavior of density with increasing temperature is shown in Fig. 8.

3.4. Magnetic measurements

Fig. 5 shows the hysteresis loops for $BaCo_2Fe_{16}O_{27}$ at different temperatures and various magnetic properties such as coercivity (H_C) and maximum magnetization (M) values measured at 8 kOe were calculated. The shape and the width of the hysteresis loop depend on factors such as chemical composition, cation distribution, porosity, and grain size. It is clear from the figure that the magnetization did not saturate but increases continuously up to 8 kOe. The reason for this is that the maximum magnetic field (8 kOe) of VSM used in present study was below the value of anisotropy field (11–13 kOe) of W-hexaferrites [21]. The loops are wide having large value of coercivity in the range of 210.61–1602.6 Oe (Table 1). Previously it was reported that the coercivity values for cobalt substituted hexaferrites determined by various research workers lie in the range of 50–200 Oe [22,23] but in the investigated ferrites we have obtained the H_C value up to 1602 Oe, which is much higher than that of the previously reported values. For

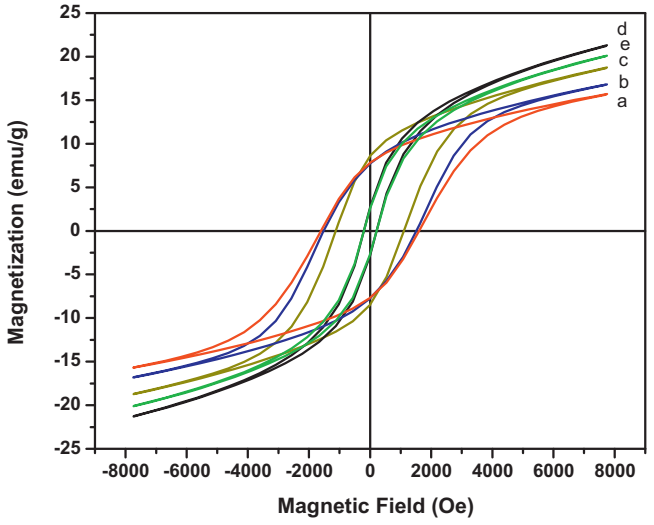

Fig. 5. M–H loops of $BaCo_2Fe_{16}O_{27}$ powders sintered at different temperatures (a = 1000 °C, b = 1050 °C, c = 1100 °C, d = 1150 °C, e = 1200 °C).

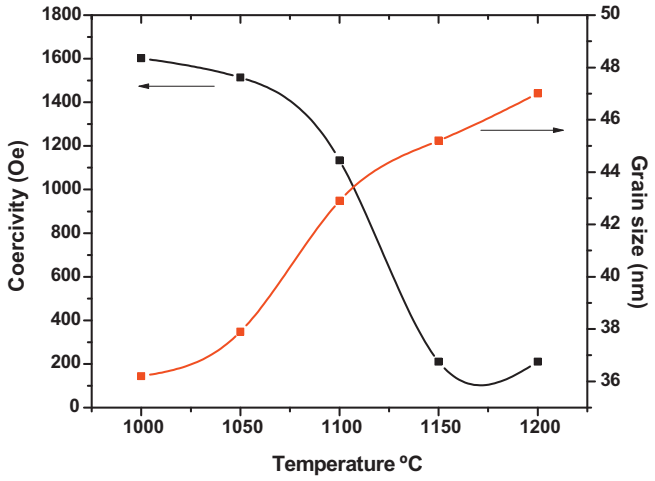

Fig. 6. Variation of grain size and coercivity with increasing temperature.

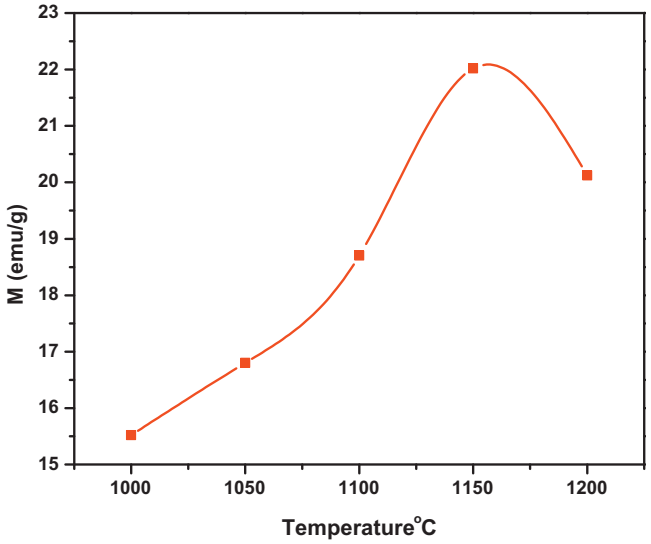

Fig. 7. Variation of magnetization values (M) with increasing temperature.

nano crystalline materials, the coercivity is closely related to the grain size 'D' of the materials depending on the exchange length L_{ex}. For 'D' greater than L_{ex}, H_C varies inversely with the grain size ($1/D$) and for Fe based alloys, L_{ex} is estimated to be 35 nm [24]. It is reported before incase of $BaCoZnFe_{16}O_{27}$ [22] that L_{ex} may be much smaller than 35 due to the small values of exchange constant and large value of magneto-crystalline anisotropy constant. Consequently, the same assumption holds for the investigated $BaCo_2Fe_{16}O_{27}$ ferrites with the grain sizes in the range of 36–47 nm, which are larger than the exchange length. Hence, it could be concluded that in our case the variations in the coercivity are due to the grain size of the hexaferrite nano particles. The behavior of coercivity and grain size with varying sintering temperature is shown in Fig. 6.

Fig. 7 represents the effect of sintering temperature on the maximum magnetization (M) values of the synthesized barium hexaferrites. It is obvious that the M continuously increases with temperature increment and the maximum value is obtained at 1150 °C followed by a decrease with further increase of temperature. The lowering of M values at higher temperature may be a consequence of larger particle size formed as a result of their coalescence with each other. It is well known that particle size has a significant effect on the magnetic properties of the magnetic materials. When the particles are smaller than the critical single domain size they are mainly in single domain. On the contrary, when the particle size becomes bigger than the critical value most of them would exist in multi-domain. With an increase in the sintering temperature the particle size also increases towards the critical single domain size. As a result, the magnetization (M) increases eventually reaching a maximum value at single domain size because of the coherent rotation of spins. As the particles become larger than the single domain size at higher temperature, the value of magnetization begins to decrease. Similar results are reported in the early literature for pure barium hexaferrites [25]. The values of magnetization (M) with varying sintering temperatures are listed in Table 1. There are few examples in which the magnetization values increased and at the same time the coercivity decreased with increment of temperature in barium W-hexaferrites. The recording media requires high enough coercivity above 600 Oe and magnetization values as high as possible [14]. On the basis of these results, it can be affirmed that coercivity (at certain temperatures) as well as saturation magnetization of the investigated ferrites can be controlled greatly by sintering temperature to use them for applications in recording media. Magnetic moment as a function of temperature was also calculated for the synthesized ferrites from the magnetization data [26] by the formula:

$$N_B(\mu_B) = \frac{M_w \times M}{5.585} \times d_B \quad (5)$$

where M_w is the molecular weight of the samples, M the magnetization values and d_B is the measured density of the samples. It is clear from Table 1 that the value of magnetic moment increases with the increase in temperature and then decreases at 1200 °C. The increase in the magnetic moment value is due to the increment in magnetization and vice versa as the magnetic moment and magnetizations are directly related to each other. The magnetization and magnetic moment data are in agreement with each other [27].

3.5. DC electrical measurements

The variation of dc electrical resistivity with increasing sintering temperature is shown in Fig. 8. It is clear that resistivity deceases monotonously with rise in sintering temperature, reaches its minimum at 1150 °C and begins to rise at higher temperature (1200 °C). This behavior can be explained on the basis of two facts, firstly at high temperatures, ferrite is deoxidated and part of Fe^{3+} ions change to Fe^{2+} ions due to conversion of Co^{2+} into Co^{3+}. During cooling, Fe^{2+} ions in the grain cannot be oxidated entirely. Electronic transfer between Fe^{3+} and Fe^{2+} is the main electric conduction mechanism of ferrite. Co^{2+} may restrain the formation of

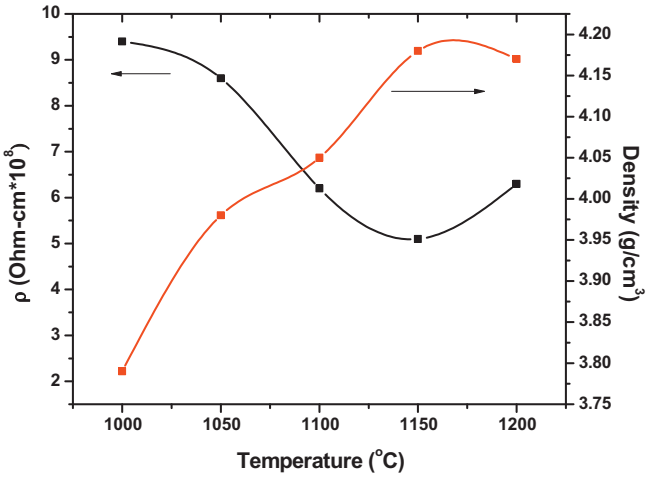

Fig. 8. Variation of resistivity and density with increasing temperature.

Fe^{2+}, which can be expressed by the well known reaction as:

$$Co^{3+} + Fe^{2+} \rightarrow Co^{2+} + Fe^{3+}$$

In addition, the active energy of electronic transfer between Co^{3+} and Co^{2+} is much higher than that of between Fe^{3+} and Fe^{2+}. As a result, resistivity of the ferrite is enhanced after being sintered at higher temperatures. If the sintering temperature is relatively low (<1150 °C), few Fe^{3+} ions change to Fe^{2+}. The inhibition of Co^{2+} on the formation of Fe^{2+} becomes a minor factor for the electric conduction of ferrite. The electronic transfer between Co^{3+} and Co^{2+} results in the rise of electric conduction. Secondly, as discussed above that density of the investigated ferrites increases with increase in temperature and reaches its maximum at 1150 °C followed by the decrease at 1200 °C. Since density is inversely related to the porosity of ferrites which may affect the dc resistivity. At lower temperatures, there may be a small number of pores which offer a little hindrance to the hopping of charge carriers between Fe^{3+} and Fe^{2+} sites thereby decreasing the resistivity of these ferrites. But at higher temperature, there will be an increased number of pores which in turn hinders the motion of charge carriers [28] and as a result resistivity increases.

4. Conclusion

Nanocrystalline and single phase $BaCo_2Fe_{16}O_{27}$ hexaferrite powders were successfully synthesized by the sol–gel auto-combustion method. Pure nanocrystalline W-type hexaferrite powders can be achieved when the as-prepared powder is sintered at and above 1000 °C. The study of IR spectra of sintered powder shows two absorption bands in the range of 430–590 cm^{-1} which are typical for hexaferrites. The grain size increases with temperature from 36 to 47 nm which is less than 50 nm and suitable to obtain high signal-to-noise ratio in high density recording media. VSM measurements show that the coercivity and magnetization values are strongly dependent on sintering temperature and have suitable values at certain temperature to make these materials promising candidates for applications in high density recording media.

Acknowledgement

Mukhtar Ahmad is highly thankful to Higher Education Commission (HEC) of Pakistan for financial support under Indigenous 5000 scholarship scheme.

References

[1] K.M. Batoo, S. Kumar, C.G. Lee, Influence of Al doping on electrical properties of Ni–Cd nano ferrites Alimuddin, Curr. Appl. Phys. 9 (2009) 826–832.
[2] V. Verma, S.P. Gairola, M.C. Mathpal, S. Annapoorni, R.K. Kotnala, Magnetic and electrical properties of manganese and cadmium co-substituted lithium ferrites, J. Alloys Compd. 481 (2009) 872–876.
[3] V. Verma, R.K. Kotnala, V. Pandey, P.C. Kothari, L. Radhapiyari, B.S. Matheru, The effect on dielectric losses in lithium ferrite by cerium substitution, J. Alloys Compd. 466 (2008) 404–407.
[4] A. Kale, S. Gubbala, R.D.K. Misara, Magnetic behavior of nanocrystalline nickel ferrite synthesized by the reverse micelle technique, J. Magn. Magn. Mater. 277 (3) (2004) 350–358.
[5] C. Kittle, Phys. Rev. 70 (1946) 965.
[6] I.S. Jacobs, C.P. Bean, in: G.T. Rado, H. Suhl (Eds.), Magnetism III, Acad. Press, NY, 1963 (Chapter 6, and references therein).
[7] J. Baszynski, Ferrites Proc. Int. Conf. Ferrites Japan 3 (1980) 212.
[8] M. Guyot, T. Merceron, M. Raibut, Ferrite Proc. Int. Conf. Ferrites Japan 3 (1980) 204.
[9] Y. Yang, B.S. Zhang, W.D. Xu, Y.B. Shi, N.S. Zhou, H.X. Lu, Microwave absorption studies of W-hexaferrite prepared by co-precipitation/mechanical milling, J. Magn. Magn. Mater. 265 (2003) 119.
[10] A.M. Abo El Ata, M.K. El Nimr, D. El Kony, A.H. AL-Hammadi, Dielectric and magnetic permeability behavior of $BaCo_{2-x}Ni_xFe_{16}O_{27}$ W-type hexaferrites, J. Magn. Magn. Mater. 204 (1999) 36.
[11] C. Šurig, K.A. Hempel, R. Müller, K.A. Görnert, Investigations on $Zn_{2-x}Co_x$W-type hexaferrite powders at low temperatures by ferromagnetic resonance, J. Magn. Magn. Mater. 150 (1995) 270.
[12] H.J. Zhang, X. Yao, L.Y. Zhang, The preparation and microwave properties of $BaZn_{2-z}Co_zFe_{16}O_{27}$ ferrite obtained by a sol–gel process, Ceram. Int. 28 (2002) 171.
[13] X.H. Wang, T.L. Ren, L.Y. Li, L.S. Zhang, Preparation and magnetic properties of $BaZn_{2-x}Co_xFe_{16}O_{27}$ nanocrystalline powders, J. Magn. Magn. Mater. 184 (1998) 95.
[14] M.J. Iqbal, M.N. Ashiq, P.H. Gomez, J.M. Munoz, Influence of annealing temperature and doping rate on the magnetic properties of Zr–Mn substituted Sr-hexaferrite nanoparticles, J. Alloys Compd. 500 (2010) 113–116.
[15] Z.X. Yue, J. Zhou, L.T. Li, H.G. Zhang, Z.L. Gui, Synthesis of nanocrystalline NiCuZn ferrite powders by sol–gel auto-combustion method, J. Magn. Magn. Mater. 208 (2000) 55.
[16] A.K. Ghatage, S.C. Choudhari, S.A. Patil, X-ray, infrared and magnetic studies of chromium substituted nickel ferrite, J. Mater. Sci. Lett. 15 (1996) 1548–1550.
[17] X. Wang, D. Li, L. Lu, X. Wang, Synthesis of substituted M- and W-type barium ferrite nanostructured powders by stearic acid gel method, J. Alloys Compd. 237 (1996) 45–48.
[18] B.D. Cullity, Elements of X-ray Diffraction, 102, Adisn Wesley Publishing Company, 1977„ p. 338.
[19] D.M. Hemeda, O.M. Hemeda, Electrical, structural, magnetic and transport properties of $Zn_2BaFe_{16}O_{27}$ doped with Cu^{2+}, J. Magn. Magn. Mater. 320 (2008) 1557–1562.
[20] I. Khan, I. Sadiq, M.N. Ashiq, M.U. Rana, Role of Ce–Mn substitution on structural, electrical and magnetic properties of W-type strontium hexaferrites, J. Alloys Compd. 509 (2011) 8042–8046.

[21] D. Lisjak, A. Znidarsic, A. Sztanislav, M. Drofenik, A two step synthesis of NiZn-W hexaferrites, J. Eur. Ceram. Soc. 28 (2008) 2057–2062.
[22] M.J. Iqbal, R.A. Khan, S. Mizukami, T. Miyazaki, Tailoring of structural, electrical and magnetic properties of $BaCo_2W$-type hexaferrites by doping with Zr–Mn binary mixtures for useful applications, J. Magn. Magn. Mater. 323 (2011) 2137–2144.
[23] Y.P. Wu, C.K. Ong, G.Q. Lin, Z.W. Li, Improved microwave magnetic and attenuation properties due to the dopant V_2O_5 in W-type barium ferrites, J. Phys. D: Appl. Phys. 39 (2006) 2915–2919.
[24] G. Herzer, Grain size dependence of coercivity and permeability in nanocrystalline ferromagnets, IEEE Trans. Magn. 26 (1990) 1397–1402.
[25] N. Kishan Reddy, V.N. Mulay, Magnetic properties of W-type ferrites, Mater. Chem. Phys. 76 (2002) 75–77.
[26] M.J. Iqbal, M.N. Ashiq, P.H. Gomez, J.M. Munoz, Magnetic, physical and electrical properties of Zr–Ni-substituted co-precipitated strontium hexaferrite nanoparticles, Scr. Mater. 57 (2007) 1093.
[27] M.N. Ashiq, M.J. Iqbal, I.H. Gul, Effect of Al–Cr doping on the structural, magnetic and dielectric properties of strontium hexaferrite nanomaterials, J. Magn. Magn. Mater. 323 (2011) 259–263.
[28] A.A. Sattar, H.M. El-sayed, K.M. El-Shokofy, M.M. el- Tabey, The effect of Al-substitution on structure and electrical properties of Mn–Ni–Zn ferrites, J. Mater. Sci. 40. (2005) 4873–4879.